

# Travelling waves and impact-parameter correlations

S. Munier,<sup>1</sup> G. P. Salam,<sup>2</sup> and G. Soyez<sup>3</sup>

<sup>1</sup>*Centre de physique théorique, École Polytechnique, CNRS, Palaiseau, France*

<sup>2</sup>*LPTHE, UPMC Univ. Paris 6, Université Paris Diderot (Paris 7), CNRS UMR 7589, Paris, France*

<sup>3</sup>*Brookhaven National Laboratory, Building 510, Upton, NY 11973, USA*

(Dated: October 29, 2018)

It is usually assumed that the high-energy evolution of partons in QCD remains local in coordinate space. In particular, fixed impact-parameter scattering is thought to be in the universality class of one-dimensional reaction-diffusion processes as if the evolutions at different points in the transverse plane became uncorrelated through rapidity evolution. We check this assumption by numerically comparing a toy model with QCD-like impact-parameter dependence to its exact counterpart with uniform evolution in impact-parameter space. We find quantitative differences, but which seem to amount to a mere rescaling of the strong coupling constant. Since the rescaling factor does not show any strong  $\alpha_s$ -dependence, we conclude that locality is well verified, up to subleading terms at small  $\alpha_s$ .

## I. INTRODUCTION

Recently, equations describing evolution towards high energy in QCD, including saturation effects [1, 2, 3, 4, 5, 6], have been proven [7] to belong to the universality class of the Fisher-Kolmogorov-Petrovsky-Piscounov (FKPP) equation. It has also been realised [8] that additional contributions were to be included in order to fully satisfy unitarity, in particular, in a way consistent with boost-invariance. Though only some partial results exist for a more complete set of evolution equations [9, 10, 11], the evolution of partonic states and their scattering at high energy is conjectured [12] to be a process of the reaction-diffusion type. The QCD evolution equations are thus thought to belong to the universality class of the stochastic FKPP (sFKPP) equation [13] which reads

$$\partial_t u(t, x) = \partial_x^2 u(t, x) + u(t, x) - u^2(t, x) + \epsilon \sqrt{2(u(t, x) - u^2(t, x))} \nu(t, x) \quad (1)$$

where  $\nu$  is a normal Gaussian noise uncorrelated in space and time;  $t$  corresponds to the rapidity variable in QCD (or the logarithm of the energy), and  $x$  is the logarithm of the transverse scale (momentum or distance) relevant to characterise the partons in the considered process, while  $\epsilon$ , the strength of the noise, is of the order of the strong coupling constant  $\alpha_s$ ;  $u$  can be thought of an event-by-event scattering amplitude, whose average over events is the physical amplitude. Such an equation is supposed to hold at a specific impact parameter.

A convenient picture for high-energy scattering is the colour dipole model [14], whose numerical implementation in terms of Monte-Carlo code event generators [15, 16, 17, 18] has been particularly useful to investigate saturation issues in QCD. The picture is the following: a hadron may be represented as a set of dipoles at the time of the interaction, which is constructed by successive dipole splittings (*i.e.* emissions of gluons in the large- $N_c$  approximation) and mergings (or any other nonlinear process that would tame the growth of their number) whose probabilities are computed from QCD

vertices. The set of dipoles resulting from this process eventually interacts with a target by exchanging gluons.

One condition for the one-dimensional<sup>1</sup> sFKPP equation to be relevant to high energy scattering is that the evolution remains local in impact parameter: indeed, if this was not the case, then correlations between different points in impact-parameter space would invalidate one-dimensional equations like (1) in QCD. At first sight, it is not at all obvious that this condition should hold: the dipole evolution kernel is singular and allows for splittings into areas that lie very far from each other in coordinate space. This nonlocal behaviour may *a priori* cause migrations of the dipole chains of successive splittings over large distances in the transverse plane, which in turn may induce correlations between different impact parameters.

In Ref. [12], this independence of the different impact parameters was assumed on the basis of a simple analytical estimate of the mean number of dipoles produced collinearly. Capturing the full complexity of the QCD evolution to achieve a more precise understanding still seems out of reach of an analytical approach. On the other hand, to our knowledge, all recent numerical studies of high-energy scattering at saturation (including gluon-number fluctuations) and its relation to the sFKPP equation (see *e.g.* [19, 20]) relied on the one-dimensional approximation.

Our goal in this paper is to test the validity of a one-dimensional formulation such as Eq. (1) in a model that has impact-parameter dependence and that we shall study numerically. We could consider the full colour dipole model and use the already-existing Monte-Carlo code in Ref. [16], but its non trivial 2-dimensional impact-parameter structure makes it far too complex to handle, especially since we want to run the evolution over a time

---

<sup>1</sup> Through this paper, by *one-dimensional* we refer to models with a single spatial dimension (*e.g.* the dipole size), in addition to the evolution variable (*e.g.* time or rapidity).

long enough to observe the asymptotic properties. Instead, we shall build a simpler model, with discretised dipole sizes and a single dimension of impact parameter, which reproduces the main features of full QCD as far as the singularities are concerned.

The structure of the paper is as follows. Sec. II recalls the essential features of the colour dipole model and its interpretation in a statistical mechanics language. In Sec. III we construct a toy model which incorporates an impact-parameter dependence, at variance with existing models of QCD evolution. We also introduce a corresponding model without impact parameter which would be fully equivalent to the first one in the absence of correlations in impact parameter. Finally, in Sec. IV, we present the numerical results on travelling waves and their impact-parameter correlations obtained within this model and compare with the model without impact parameter dependence.

## II. ANALYTICAL PRELIMINARIES

### A. Scattering in the dipole model

In the colour dipole model [14], high-energy evolution is viewed in the following way. Two hadrons (which are asymptotically sets of colourless  $q\bar{q}$  dipoles, for the simplicity of the argument) develop under rapidity evolution highly occupied Fock-states which themselves may be seen as collections of colour dipoles. The building up of the states of each hadron is specified by providing the splitting rate of a dipole whose endpoints have transverse coordinates  $(x_0, x_1)$  into two dipoles  $(x_0, x_2)$  and  $(x_1, x_2)$  as the result of a gluon emission at position  $x_2$ . It reads [14]

$$\frac{dP}{d(\bar{\alpha}y)}(x_{01} \rightarrow x_{02}, x_{12}) = \frac{x_{01}^2}{x_{02}^2 x_{12}^2} \frac{d^2 x_2}{2\pi}. \quad (2)$$

This splitting process is actually supplemented by a saturation mechanism, which limits the local density of dipoles to about  $1/\alpha_s^2$ . Unfortunately, it has not been formulated in the dipole model. (For a study of the problems that one has to face to incorporate saturation effects in this framework, see *e.g.* Ref. [21]). It is sometimes seen as a progressive slowing down of the dipole emission rate once the local density is of the order of  $1/\alpha_s^2$  [5, 22]. It could also be recombination of dipoles, which corresponds to the reabsorption of gluons [21], or some form of colour reconnection (“swings”) among the constituent gluons of the dipoles [18]. But the very nature of the mechanism is not crucial to our discussion, and when building our toy model, we pick the simplest one to implement numerically.

At the time of the interaction, pairs of dipoles made of one dipole from the left-moving hadron and one dipole from the right-moving hadron, may exchange gluons, provided that they are of similar sizes and sit at the same

impact parameter. It is actually simpler to think of the process in the rest frame of one of the hadrons: then, only the moving hadron (the probe) undergoes evolution, while the other one (the target) remains in its bare asymptotic state.

We need to clarify what is meant by two dipoles sitting at the same impact parameter (up to a distance of the order of their size). When a highly evolved hadron is probed by an elementary dipole of size  $x_{01} = x_0 - x_1$ , the scattering amplitude  $T$  is related to the density  $n$  in the following way:

$$T(y, x_{01}, \frac{x_0+x_1}{2}) = \frac{\pi^2 \alpha_s^2}{2} \times \int \frac{d^2 z_0}{2\pi} \frac{d^2 z_1}{2\pi} \times \log^2 \frac{|x_0 - z_1|^2 |x_1 - z_0|^2}{|x_0 - z_0|^2 |x_1 - z_1|^2} n(y, z_{01}, \frac{z_0+z_1}{2}), \quad (3)$$

where the summation goes over the positions of the dipoles in the Fock state of the evolved hadron. The first argument of  $T$  is the rapidity, the second one the dipole size and the last one the impact parameter. This formula means that  $T$  roughly counts the dipoles which have a size of the order of  $|x_{01}|$  and sit in a region of impact parameter delimited by a circle of radius  $|x_{01}|$  around the position (or impact parameter)  $(x_0 + x_1)/2$ .

From the dipole splitting probability (2), we can infer the evolution equation for  $T$ . The simplest version of this equation is obtained when the target is a very large nucleus, that is, made of a large (formally infinite) number of bare dipoles. One gets

$$\begin{aligned} \partial_{\bar{\alpha}y} T(y, x_{01}, \frac{x_0+x_1}{2}) &= \int \frac{d^2 x_2}{2\pi} \frac{x_{01}^2}{x_{02}^2 x_{12}^2} \left[ T(y, x_{02}, \frac{x_0+x_2}{2}) \right. \\ &\quad + T(y, x_{12}, \frac{x_1+x_2}{2}) - T(y, x_{01}, \frac{x_0+x_1}{2}) \\ &\quad \left. - T(y, x_{02}, \frac{x_0+x_2}{2}) T(y, x_{12}, \frac{x_1+x_2}{2}) \right] \quad (4) \end{aligned}$$

This is the well-known Balitsky-Kovchegov (BK) equation [3, 4]. Its linear part is the Balitsky-Fadin-Kuraev-Lipatov (BFKL) equation [23], while its nonlinear part accounts for multiple scattering on the dense target. For a general target, additional unitarity effects must be taken into account [8, 12], and the corresponding equation is not yet fully known, though some partial results covering the main features are available [9, 10, 11, 24]. For example, at large- $N_c$  and in the two-gluon-exchange approximation, it has been shown [9] that (4) has to be supplemented by a non-local noise term taking into account the gluon-number fluctuations when the target is dilute.

### B. Travelling waves

Recent research has established a link between high energy QCD evolution and reaction-diffusion processes. Indeed, the Balitsky-Kovchegov equation at fixed impact

parameter, in the diffusive approximation<sup>2</sup>, was shown to be identical to the FKPP equation [7]. Moreover, as recalled in the Introduction, it is thought that full high-energy QCD beyond the approximations assumed to establish the BK equation lies in the universality class of reaction-diffusion processes [12]. The stochastic version of the FKPP equation (see Eq. (1)) then becomes relevant, with a noise term of the order of the strong coupling constant  $\alpha_s$ . The interesting outcome of this correspondence consists in universal results for the scattering amplitudes that can be analytically computed in the asymptotic regime of very small  $\alpha_s$  and large rapidities though, for larger values of the coupling, the same behaviours are observed numerically [19, 20, 22]. Even if the precise form of the evolution equations are not fully known, all the models presented so far have shown the same asymptotic properties.

Generally speaking, equations of the form (4) admit travelling wave solutions in the variable  $\log(1/x_{01}^2)$  when the dependency upon the impact parameter is ignored. The main features of these waves only depend on the Mellin moments  $\chi(\gamma)$  of the splitting probability (2). These solutions are attractors in the sense that a large class of initial conditions (actually all initial conditions that are physical for the considered processes) converge to them at large rapidity. The position  $\rho_s(y) \equiv \log Q_s^2(y)$  of the wave defines the saturation scale  $Q_s(y)$ . Thus, the saturation scale and its rapidity dependence emerge naturally from the travelling-wave solutions. At large rapidities, the speed of the wave  $\partial_{\bar{\alpha}y}\rho_s(y)$  is [1, 25, 26]

$$V = \frac{\chi(\gamma_c)}{\gamma_c} \quad (5)$$

where  $\gamma_c$  satisfies

$$\chi'(\gamma_c) = \frac{\chi(\gamma_c)}{\gamma_c}. \quad (6)$$

The wave front decays exponentially in the small- $|x_{01}|$  region like

$$T \sim \exp\left(-\gamma_c \log \frac{1}{x_{01}^2 Q_s^2(y)}\right). \quad (7)$$

Geometric scaling [27] is the physical phenomenon that corresponds to the fact that the amplitude only depends on the combination  $x_{01}^2 Q_s^2(y)$  rather than on each variable separately.

If stochasticity is taken into account, then the properties of the solutions are modified. The travelling waves become noisy, corresponding to the fact that each individual event is made of a discrete number of dipoles introducing fluctuations important in the tail of the front

where the dipole density is of order 1 (or,  $T \sim \alpha_s^2$ ). The logarithm of the squared saturation scale acquires a variance that grows linearly with rapidity. The velocity of the fronts, that is to say, the rates of growth of  $\log Q_s^2(y)$  averaged over the realisations, reach an asymptotic value smaller than that coming out of the BK equation by a shift proportional to  $1/\log^2(1/\alpha_s^2)$ . The physical scattering amplitude is obtained by averaging over events, and gets tilted [28] with respect to what it would be if the BK equation held. Geometric scaling is broken [8] and replaced by diffusive scaling [8, 9, 12]:

$$\langle T \rangle = \text{erfc} \left[ \frac{\log(x_{01}^2 Q_s^2(y))}{\sqrt{\bar{\alpha}y / \log^3(1/\alpha_s^2)}} \right], \quad (8)$$

which reflects the fact that the variance of the front position scales like  $\bar{\alpha}y / \log^3(1/\alpha_s^2)$ .

It is important to note that the wave velocity gets closer to the mean-field result (5) when  $\alpha_s$  decreases, and not surprisingly, the variance of the front position gets smaller in the same limit, which is the sign that fluctuations get milder. This limit corresponds to large maximum local densities of dipoles, for which statistical fluctuations are indeed expected to vanish, and thus a mean-field approximation may indeed be justified.

These results are believed to be rigorously true for one-dimensional models of reaction-diffusion type. Their extension to QCD actually relies in particular on the postulate that the impact-parameter variable does not play a role in equations such as (4) and in their stochastic extensions, for the latter should be “local” enough. However, this fundamental assumption has never been checked, and this is precisely what we intend to do numerically in this paper. Before we turn to this task (Sec. III), let us recall the arguments in favour of the decoupling of the travelling waves at different impact parameters.

### C. Picture of the evolution including impact parameter

Let us start with a single dipole at rest, and bring it gradually to a higher rapidity. During this process, this dipole may be replaced by two new dipoles, which themselves may split, and so on, eventually producing a chain of dipoles. Figure 1 pictures one realization of such a chain.

According to Eq. (2), splittings to smaller-size dipoles are favoured, and thus, one expects that the sizes of the dipoles get smaller on the average, and that in turn, the successive splittings become more local. The dipoles around region “1” and those around region “2” should have an independent evolution beyond the stage pictured in the figure: further splittings will not mix in impact parameter space, and thus, the travelling waves around these regions should be uncorrelated. For a dipole in region 1 of size  $r$  to migrate to region 2, it should first

<sup>2</sup> The *diffusive approximation* corresponds to expanding the BFKL kernel to second order.

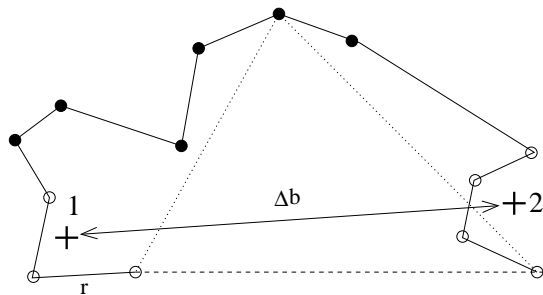


FIG. 1: Sample dipole configuration in impact-parameter space. The points represent the gluons, and the line is the dipole chain after evolution. The initial dipole is represented by a dashed line, and the first splitting by two dotted lines. For the two impact parameters denoted by a “+” sign (labelled 1 and 2) their further respective evolutions are believed to be uncorrelated. The dipoles whose both endpoints are empty circles are those which are seen at these peculiar impact parameters. For clarity, we have omitted the large number of tiny dipoles produced at every endpoints.

split into a dipole whose size is of the order of the distance  $\Delta b$  between regions 1 and 2, up to a multiplicative uncertainty of order 1. (We assume in this discussion that the dipoles in region 2 relevant to the propagation of the local travelling waves, that is, those which are in the bulk of the wave front, also have sizes of order  $r$ ). Roughly speaking, the rate of such splittings may be estimated from the dipole splitting probability (2): it is of order  $\bar{\alpha}(r^2/(\Delta b)^2)^2$ , while the rate of splittings of the same dipole into a dipole of similar size in region 1 is of order  $\bar{\alpha}$ . Thus the first process is strongly suppressed as soon as regions 1 and 2 are more distant than a few units of  $r$ . Note that for  $\Delta b \gtrsim 1/Q_s$ , saturation may further reduce the emission of the first, large, dipole leading to an even stronger suppression of the estimated rate.

There is a second case that we should worry about. What could also happen is that some larger dipole has, by chance, one of its endpoints tuned to the vicinity of the coordinate one is looking at (at a distance which is at most  $|\Delta r| \ll 1/Q_s(Y)$ ), and easily produces a large number of dipoles there. In this case, the position of the travelling wave at that impact parameter would suddenly jump. If such events were frequent enough, then they would modify the average wave velocity and thus the one-dimensional picture. We may give a rough estimate of the rate at which dipoles of size smaller than  $\Delta r$  are produced. Assuming local uniformity for the distribution of the emitting dipoles, the rate (per unit of  $\bar{\alpha}y$ ) of such events can be written

$$\int_{r_0 > \Delta r} \frac{d^2 r_0}{r_0^2} \int_{\varepsilon < \Delta r} d^2 \varepsilon n(r_0) \left(\frac{\varepsilon}{r_0}\right)^2 \frac{1}{2\pi} \frac{r_0^2}{\varepsilon^2 (r_0 - \varepsilon)^2}, \quad (9)$$

where we integrate over large dipoles of size  $r_0 > \Delta r$  emitting smaller dipoles (of size  $\varepsilon < \Delta r$ ) with a probability  $d^2 \varepsilon r_0^2 / (2\pi \varepsilon^2 (r_0 - \varepsilon)^2)$ . The factor  $(\varepsilon/r_0)^2$  accounts for the fact that one endpoint of the dipole of size  $r_0$  has

to be in a given region of size  $\varepsilon$  in order to emit the dipoles at the right impact parameter. To estimate this expression, we first use  $n(r_0) = T(r_0)/\alpha_s^2$  and use for  $T$  the simplified expression

$$T(r_0) = \Theta(r_0 - 1/Q_s) + (r_0^2 Q_s^2)^{\gamma_c} \Theta(1/Q_s - r_0),$$

which splits the front into a saturated region ( $r_0 > 1/Q_s$ ) and a tail with geometric scaling ( $r_0 < 1/Q_s$ ). Using  $r_0 - \varepsilon \approx r_0$  in the emission kernel, the integration is then easily performed and one finds a rate whose dominant term is

$$\frac{\pi}{2\alpha_s^2} \frac{((\Delta r)^2 Q_s^2)^{\gamma_c}}{1 - \gamma_c}. \quad (10)$$

For  $(\Delta r)^2 \ll (\alpha_s^2)^{1/\gamma_c} / Q_s^2$ , that is, ahead of the bulk of the front, this term is parametrically less than 1 and is in fact of the order of the probability to find an object in this region that contributes to the normal evolution of the front [29]. Hence there is no extra contribution due to the fact that there are many dipoles around at different impact parameters.

However, it seems difficult to perform a precise calculation of these effects beyond order-of-magnitude estimates, and anyway, this average picture may be spoiled by the statistical event-by-event fluctuations. So, we do not have any insight on how to estimate more precisely this effect analytically. It is thus important to perform a numerical simulation and check the correlations of travelling waves at different impact parameters.

### III. CONSTRUCTION OF THE MODEL

#### A. Simplified model with impact-parameter dependence

##### 1. Fock state evolution

In order to arrive at a model that is tractable numerically, we only keep one transverse dimension instead of two in 3+1-dimensional QCD. However, we cannot consider genuine 2+1-dimensional QCD because we do not wish to give up the logarithmic collinear singularities at  $x_2 = x_0$  and  $x_2 = x_1$ . Moreover, QCD with one dimension less has very different properties at high energies [30]. A splitting rate which complies with our requirements is:

$$\frac{dP}{d(\bar{\alpha}y)} = \frac{1}{4} \frac{|x_{01}|}{|x_{02}||x_{12}|} dx_2. \quad (11)$$

We can further simplify this probability distribution by keeping only its collinear and infrared asymptotics (as in [31]). If  $|x_{02}| \ll |x_{01}|$  (or the symmetrical case  $|x_{12}| \ll |x_{01}|$ ), the probability reduces to  $dx_2/|x_{02}|$  ( $dx_2/|x_{12}|$  resp.). The result of the splitting is a small dipole  $(x_0, x_2)$  together with one close in size to the parent. So for simplicity we will just add the small dipole to the system

and leave the parent unchanged. In the infrared region, a dipole of size  $|x_{02}| \gg |x_{01}|$  is emitted with a rate given by the large- $|x_{02}|$  limit of the above probability. The probability laws (2),(11) imply that a second dipole of similar size should be produced while the parent dipole disappears. To retain a behaviour as close as possible to that in the collinear limit, we will instead just generate a single large dipole and maintain the parent. To do this consistently one must include a factor of two in the infrared splitting rate, so as not to modify the average rate of production of large dipoles.

In formulating our model precisely, let us focus first on the distribution of the sizes of the participating dipoles. (The simplifying assumptions made above enable one to choose the sizes and the impact parameters of the dipoles successively). We call  $r$  the modulus of the emitted dipole,  $r_0$  the modulus of its parent and  $Y = \bar{\alpha}y$ . The splitting rate (11) reads, in this simplified model

$$\frac{dP_{r_0 \rightarrow r}}{dY} = \theta(r - r_0) \frac{r_0 dr}{r^2} + \theta(r_0 - r) \frac{dr}{r}, \quad (12)$$

and the original parent dipole is kept. Logarithmic variables are the relevant ones here, so we introduce

$$\rho = \log_B(1/r) \quad \text{or} \quad r = B^{-\rho}, \quad (13)$$

where the base  $B$  will later be set to two in the actual numerical calculations. We can thus rewrite the dipole creation rate as

$$\frac{dP_{\rho_0 \rightarrow \rho}}{dY} = \theta(\rho_0 - \rho) B^{\rho - \rho_0} \log B d\rho + \theta(\rho - \rho_0) \log B d\rho. \quad (14)$$

To further simplify the model, we discretise the dipole sizes and consider a lattice in  $\rho$  with lattice spacing  $\Delta$  (which will later be set to one). This amounts to restricting the dipole sizes to negative integer powers of  $B^\Delta$ . The probability that a dipole at lattice site  $i$  (*i.e.* a dipole of size  $B^{-i\Delta}$ ) creates a new dipole at lattice site  $j$  is

$$\frac{dP_{i \rightarrow j}}{dY} = \int_{\rho_j}^{\rho_{j+1}} \frac{dP_{\rho_i \rightarrow \rho}}{dY} \quad (15)$$

$$= \begin{cases} \Delta \log B & j \geq i \\ (B^\Delta - 1)B^{(j-i)\Delta} & j < i \end{cases}. \quad (16)$$

The rates  $dP_{i\pm}/dY$  for a dipole at lattice site  $i$  to split to any lattice site  $j \geq i$  or  $j < i$  respectively are then given by

$$\frac{dP_{i+}}{dY} = \sum_{j=i}^{L-1} \frac{dP_{i \rightarrow j}}{dY} = \Delta \log B(L - i), \quad (17)$$

$$\frac{dP_{i-}}{dY} = \sum_{j=0}^{i-1} \frac{dP_{i \rightarrow j}}{dY} = 1 - B^{-i\Delta}, \quad (18)$$

where we have restricted the lattice to  $0 \leq i < L$ , for obvious reasons related to the numerical implementation.

Now we have to address the question of the impact parameter of the emitted dipole. In QCD, the collinear dipoles are produced near the endpoints of the parent dipoles. Let us take a parent of size  $r_0$  at impact parameter  $b_0$ . We set the emitted dipole (size  $r$ ) at the impact parameter  $b$  such that

$$b = b_0 \pm \frac{r_0 \pm r \times s}{2} \quad (19)$$

where  $s$  has uniform probability between 0 and 1. It is introduced to obtain a continuous distribution of the impact parameter unaffected by the discretisation of  $r$ . This prescription is quite arbitrary in its details, but the latter do not influence significantly the physical observables. Each of the two signs that appear in the above expression is chosen to be either + or - with equal weights. We apply the same prescription when the emitted dipole is larger than its parent.

## 2. Scattering amplitude

We explained before that in QCD, the scattering amplitude of an elementary probe dipole of size  $r_i = B^{-i\Delta}$  with a dipole in an evolved Fock state is proportional to the number of objects which have a size of the same order of magnitude and which sit in an area of radius of order  $r_i$  around the impact point of the probe dipole. Since in our case, the sizes are discrete, the amplitude is just given, up to a factor, by the number of dipoles that are exactly in the same bin of size as the probe, namely

$$T(i, b_0) = (\alpha_s^2/\Delta) \times \#\{\text{dipoles of size } B^{-i\Delta} \text{ at impact parameter } b \text{ such that } |b - b_0| < r_i/2\}. \quad (20)$$

## 3. Saturation

We now have to enforce unitarity, that is the condition

$$T(i, b) \leq 1 \quad (21)$$

for any  $i$  and  $b$ . This condition is expected to hold due to gluon saturation in QCD. However, saturation is not included in the original dipole model. Nevertheless, as argued in Section II, the asymptotic properties are not affected by the details on how we implement the condition (21). The simplest choice is to veto splittings that would locally drive the amplitude to values larger than 1. In practice, for each splitting that gives birth to a new dipole of size  $i$  at impact parameter  $b$ , we compute  $T(i, b)$  and  $T(i, b \pm r_i/2)$ , and throw away the produced dipole whenever one of these numbers gets larger than one.

Given the definition of the amplitude  $T$ , this saturation rule implies that there is a maximum number of objects in each bin of size and at each impact parameter, which is equal to  $N_{\text{sat}} = \Delta/\alpha_s^2$ .

#### 4. Note on the implementation

The model is now completely specified by Eqs. (16), (19), (20) and (21).

The implementation of the dipole splittings is quite straightforward, since the distribution of the sizes and impact parameters of the produced dipoles are very simple. At a given point along the rapidity evolution, we choose the dipole that is going to split next. The dipole lifetimes only depend on their sizes, and are simply given by the inverse rates  $d(P_{i+} + P_{i-})/dY$  in Eq. (18). Once this dipole has been chosen, we determine its size and impact parameter according to Eqs. (16), (19). Next, we check that the conditions for the amplitude not to violate unitarity are satisfied. If this is the case, the new dipole is integrated in the Fock state. Otherwise, the dipole is rejected.

The structure of the data has to be chosen carefully to save CPU time. Indeed, in order to compute the cross section  $T$ , one needs to search for all dipoles of a given size within a specified range of impact parameter about the probe dipole. Given that the number of dipoles grows very quickly with rapidity (a priori exponentially), it is crucial to be able to search these dipoles in a time that does not grow faster than the logarithm of their number. To meet this requirement, an array indexed by the discrete logarithmic size  $i$  of the dipoles points to binary trees of dipoles of identical sizes, ordered by their impact parameter.

The number of objects grows very fast due to the large number of tiny dipoles that may easily be produced, and consequently, the computer memory would be saturated quite early in the evolution. Imposing the above-mentioned cutoff  $L$  on the logarithmic size is not efficient enough to limit the number of objects. The reason is that  $L$  has to be taken quite high (we chose 50): if it is lower than that, the evolution gets hampered within the range of rapidity that is of interest for investigating saturation. Hence we decided to enforce a lower cutoff also on the ratio  $\kappa = B^{-i}/|b - b_N|$  of the size of each produced dipole to the distance between its impact parameter  $b$  and any impact parameter  $b_N$  at which we would measure cross sections. Imposing this cutoff, we anticipate on the fact that a small dipole very far from the impact parameters of interest has only a tiny probability to migrate back through its further splittings;  $\kappa$  has of course to be taken sufficiently small, and varied in order to evaluate its effect.

Restrictions due to machine accuracy must also be addressed. Indeed, when dipoles become small through evolution, one must be able to resolve numerically equally small distances in impact parameter. Since absolute impact parameters will be of the order of 1 and are coded on 53 significant bits (typical double precision floating point numbers), we have to limit the dipole sizes to about  $i < 53 \log B / \log 2$ . A way to overcome this limitation is to use arbitrary precision arithmetic libraries [32], but

this is both more memory and CPU costly so we tried to avoid this solution.

## B. Fixed impact-parameter version

We may now consider a similar model, but in which there is no impact-parameter dependence. We will call it ‘‘FIP’’ for Fixed Impact Parameter, while the complete model will be termed ‘‘AIP’’ (Any Impact Parameter).

### 1. Formulation

One may understand how to ‘‘remove’’ the impact parameter from the AIP model as follows. The essential point is that the interaction between the probe and target is local in impact parameter. That means that if a probe of size  $r$  is to interact with a dipole of size  $r$  in the target, then the probe should also be roughly within a transverse distance  $r$  of the target dipole. When explicit impact parameter information is maintained, one simply enforces this in one’s determination of probe-target interactions. If instead one discards the impact parameter information, then one must find another way of accounting for the fact that most target dipoles of size  $r$  will be too far from the probe to have a significant interaction with it. The simplest is to observe that the probability of a target dipole being close enough to the probe is  $r/r_0$ , where  $r_0$  is the initial size of the system. Therefore the number of dipoles of size  $r$  sufficiently close to a specific fixed impact parameter,  $n^{(f)}(r)$ , is given in terms of the total number of dipoles of size  $r$ ,  $n(r)$ , by the relation  $n^{(f)}(r) = r/r_0 n(r)$ . One may reinterpret this in terms of an FIP-specific branching probability, which relates to the normal branching probability via

$$\frac{dP_{i \rightarrow j}^{(f)}}{dY} = \frac{r_j}{r_i} \frac{dP_{i \rightarrow j}}{dY} = B^{(i-j)\Delta} \frac{dP_{i \rightarrow j}}{dY} \quad (22)$$

$$= \begin{cases} \Delta \log B B^{(i-j)\Delta} & j \geq i \\ (B^\Delta - 1) & j < i \end{cases} \quad (23)$$

It is straightforward to verify that this reproduces the condition  $n^{(f)}(r) = r/r_0 n(r)$ , and from eqs. (22,23) one then derives

$$\frac{dP_{i+}^{(f)}}{dY} = \sum_{j=i}^{L-1} \frac{dP_{i \rightarrow j}^{(f)}}{dY} = \Delta \log B \frac{1 - B^{-(L-i)\Delta}}{1 - B^{-\Delta}}, \quad (24)$$

$$\frac{dP_{i-}^{(f)}}{dY} = \sum_{j=0}^{i-1} \frac{dP_{i \rightarrow j}^{(f)}}{dY} = (B^{i\Delta} - 1) i. \quad (25)$$

Of course, the saturation rule in the FIP model is that a dipole is not produced if the number of objects of the same size is already larger than  $N_{\text{sat}}$ .

## 2. Numerical implementation

The FIP model is quite straightforward to implement. The splitting probabilities are as simple as those in the AIP model. Since again the dipoles have discrete sizes, it is enough to update an array indexed by the logarithmic dipole size  $i$ , each cell of which contains the corresponding number of dipoles.

### C. Expected properties of the amplitudes in these models

At this stage, we can derive the properties of the travelling waves. The first step is to write down the BFKL evolution of the dipole densities. If  $n_i$  is the number of dipoles at lattice site  $i$ , we have

$$\begin{aligned} \partial_Y n_i &= \sum_j \frac{dP_{j \rightarrow i}^{(f)}}{dY} n_j \\ &= \sum_{j \geq i} \Delta \log B B^{(j-i)\Delta} n_j + \sum_{j < i} (B^\Delta - 1) n_j. \end{aligned} \quad (26)$$

The amplitude  $T$  is just  $n_i/N_{\text{sat}}$ .

The equation that corresponds to the BK equation, which preserves unitarity, is obtained from the latter by taking the minimum of  $n$  as given by the linear evolution and  $N_{\text{sat}}$ , at each rapidity step and for each dipole size.

The FIP model has the same number of variables as the FKPP equation: one evolution variable and one spatial variable (which is the dipole size) in which diffusion can occur. It is a branching diffusion process in the discretised space of dipole sizes, with a saturation condition that limits the number of objects (dipoles) of each size. From a general analysis of such models, we know that the realisations of the evolution of the scattering amplitude are noisy travelling waves whose properties may be obtained from the branching diffusion kernel.

The eigenfunctions of the kernel of the fixed-impact parameter evolution are of the form  $B^{-i\gamma\Delta}$  with the corresponding eigenvalues

$$\begin{aligned} \chi(\gamma) &= \sum_{k \leq 0} \Delta \log B B^{-k\Delta} B^{k\gamma\Delta} + \sum_{k < 0} (B^\Delta - 1) B^{k\gamma\Delta} \\ &= \frac{\Delta \log B}{1 - B^{(\gamma-1)\Delta}} + \frac{B^\Delta - 1}{B^{\gamma\Delta} - 1}. \end{aligned} \quad (27)$$

Note that in the continuous limit obtained by letting  $\Delta$  go to 0, one recovers the standard collinear approximation to the BFKL kernel:

$$\chi(\gamma) = \frac{1}{\gamma} + \frac{1}{1 - \gamma}, \quad (28)$$

which confirms that we have kept the most important singularities. Furthermore, one may verify that the  $1/\gamma$  and  $1/(1 - \gamma)$  singularities are present independently of

the value of  $\Delta$ . From the expression Eq. (27) for the kernel, it is possible to find the critical parameters that control the travelling waves for the mean-field limit (*i.e.* the infinite  $N_{\text{sat}}$  limit) of the evolution with saturation. A numerical solution of the condition  $\gamma\chi'(\gamma) = \chi(\gamma)$  (for  $\Delta = 1$  and  $B = 2$ ) leads to

$$\begin{aligned} \gamma_c &= 0.69216 \dots, & \chi(\gamma_c) &= 5.2314 \dots \\ \text{and} & & \chi'(\gamma_c) &= 7.5582 \dots \end{aligned} \quad (29)$$

The travelling waves proceed to larger values of  $i$  as rapidity is increased. They are characterised by their position  $\rho_s$ , related to the saturation scale in QCD, and by the shape of their leading edge. Note that there is a certain freedom in the definition of the position of the front: we will specify our choice in Sec. IV A. The large-rapidity velocity of the wave reads

$$\frac{d\rho_s}{dY} = \frac{1}{\log B} \chi'(\gamma_c), \quad (30)$$

while the shape is given by

$$T(i) \sim B^{-\gamma_c(\Delta i - \rho_s)} \quad (31)$$

in the forward part of the wave front defined by  $i\Delta \gg \rho_s$ . For a finite  $N_{\text{sat}}$ , the velocity is in general lower, and differs from the mean-field velocity by amount of order  $1/\log^2 N_{\text{sat}}$ . Furthermore, the front position acquires a dispersion from event to event, which goes like  $Y/\log^3 N_{\text{sat}}$  asymptotically for large  $Y$  and  $N_{\text{sat}}$ .

If the property that all impact parameters evolve independently of each other is true, travelling waves with the same properties are expected for  $T(i, b)$  in the AIP model, at each value of the impact parameter. This is what we shall investigate numerically in the last section.

## IV. NUMERICAL RESULTS

We take as an initial condition a number  $N_{\text{sat}}$  of dipoles of size 1 ( $i = 0$ ), uniformly distributed in impact parameter between  $-r_0/2$  and  $r_0/2$  in the case of the AIP model. (This means that the impact parameters of the initial  $N_{\text{sat}}$  dipoles are randomly chosen according to a flat distribution<sup>3</sup>). We vary  $N_{\text{sat}}$  between 10 and 200, and the cutoff  $\kappa$  between  $10^{-1}$  and  $10^{-4}$ . The impact parameters  $b_j$  that are considered are respectively 0,  $10^{-6}$ ,  $10^{-4}$ ,  $10^{-2}$  and  $10^{-1}$ . We set  $\Delta = 1$  and  $B = 2$  in all that follows.

<sup>3</sup> We have checked that starting with a fixed initial distribution of dipoles in impact parameter leads to the same asymptotic results. See *e.g.* Fig. 8 further in this Section where the simulation for  $N_{\text{sat}} = 100$  up to  $Y = 4$  has been obtained by taking  $N_{\text{sat}}$  dipoles at  $b = 0$  as an initial condition: only differences in the pre-asymptotic regime are observed.

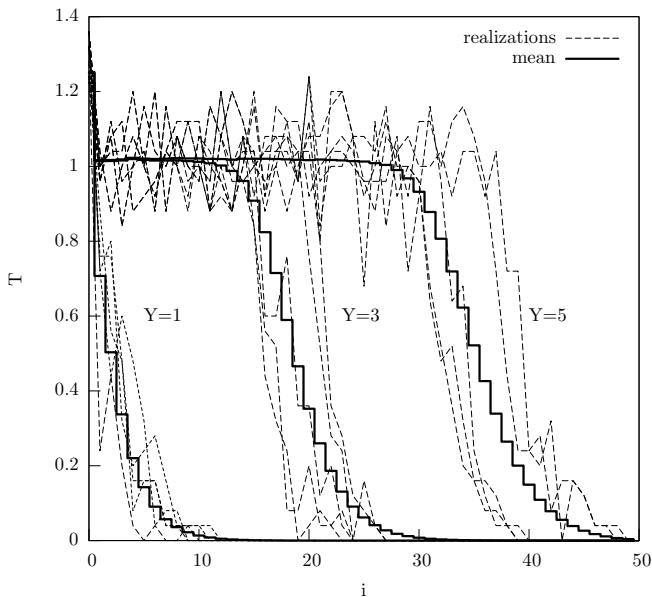


FIG. 2: Shape of the travelling-wave front in the AIP model at central impact parameter, for three rapidities ( $Y = 1, 3$  and  $5$ ). Five different events are shown in dashed lines, while the average over many events is displayed with continuous lines.  $N_{\text{sat}} = 25$  and  $\kappa = 10^{-2}$ .

The number of events generated is typically  $10^4$  for each set of parameters, which allows one to measure the average and variance of the position of the travelling waves to a sufficient accuracy.

The numerical data presented below were obtained using two independent implementations of the Monte-Carlo event generator, which gave fully consistent results.

### A. Amplitudes at a given impact parameter

For the needs of the discussion in this section, convenient values of  $N_{\text{sat}}$  and  $\kappa$  are 25 and  $10^{-2}$  respectively. The latter will be the default values, unless stated explicitly.

First, we can observe very clearly the propagation of the travelling waves, in the FIP model (not pictured) as well as in the AIP model at different impact parameters (see Fig. 2; similar curves would be obtained in the FIP model). Note that the different realisations shown in Fig. 2 sometimes overshoot 1. This is due to the fact that the unitarity constraint is only imposed at a finite number of points (in practice only 3, in order to save CPU time). Adding more points reduces the excess but does not change the final results for the wave front velocity and dispersion.

To explore quantitatively the properties of the waves, we define their position  $\rho_s$  as the largest  $i$  (*i.e.* the small-

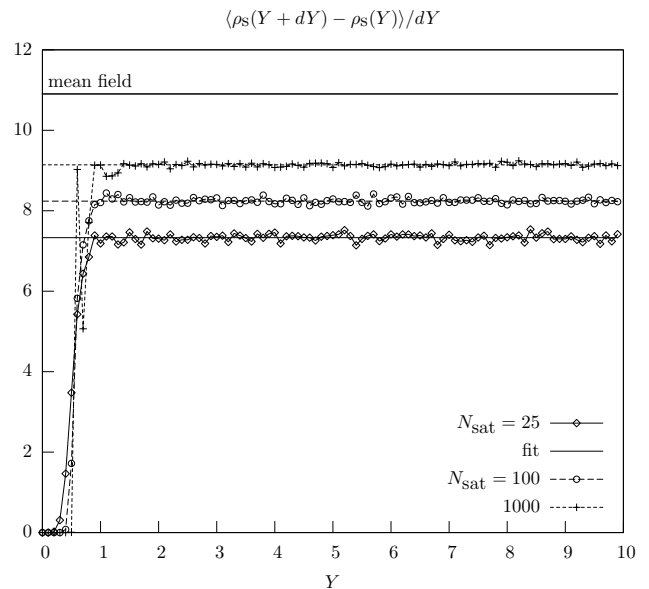


FIG. 3: Instantaneous velocity of the front in the FIP model, for  $N_{\text{sat}} = 25, 100, 1000$  as a function of the rapidity. The mean-field value of the velocity  $\chi'(\gamma_c)/\log B$  is also shown in full line.

est dipole size) for which  $T \geq 1/2$ , namely

$$N_{\text{sat}} \times T(\rho_s, b_j) \geq \frac{N_{\text{sat}}}{2} \quad (32)$$

and  $N_{\text{sat}} \times T(\rho_s + 1, b_j) < \frac{N_{\text{sat}}}{2}.$

In this section, we will be interested in measuring the  $Y$ -slope of the average of  $\rho_s$  over events, as well as the variance of the front position

$$\sigma^2(Y) = \langle \rho_s^2(Y) \rangle - \langle \rho_s(Y) \rangle^2. \quad (33)$$

First, let us address the FIP model in which there is no impact-parameter dependence. We plot the velocity of the travelling wave for different values of  $N_{\text{sat}}$  in Fig. 3, and the corresponding variance in Fig. 4, both as a function of the evolution variable  $Y$ . We see that the velocity reaches quite quickly its asymptotic regime: it becomes stable as soon as  $Y > 2$ , for any value of  $j$ . The same holds for the growth rate of the variance. A fit in the range  $2 < Y < 5$  can safely be extrapolated to  $Y > 5$ . (This remark will be useful in the case of the AIP model, where we have to restrict the calculation to  $Y < 5$  for technical reasons.) The results of the fits are shown in Tab. I, for several values of  $N_{\text{sat}}$ .

Now we repeat the same calculation in the AIP model, for  $Y < 5$ . The choice of the upper limit on  $Y$  is dictated by numerical limitations: if  $Y$  gets larger, then the travelling waves are likely to explore too small dipole sizes which cannot be resolved numerically for lack of accuracy (see Sec. III A). We first check that the front velocity is

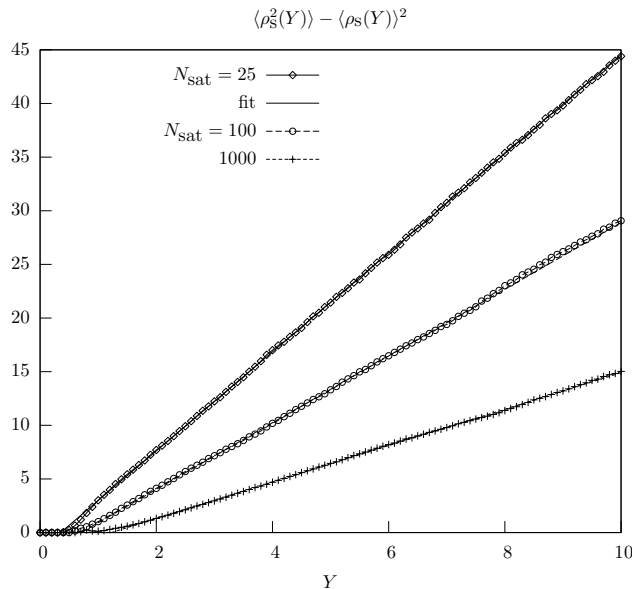


FIG. 4: Variance of the front position as a function of the rapidity in the FIP model. Three different values of  $N_{\text{sat}}$  are displayed. A linear fit is indistinguishable from the numerical data.

$N_{\text{sat}}$	$\kappa$	$\frac{d\langle \rho_s(Y) \rangle}{dY}$			$\frac{d\sigma^2}{dY}$			# events		
		FIP	$10^{-2}$	$10^{-3}$	FIP	$10^{-2}$	$10^{-3}$	FIP	$10^{-2}$	$10^{-3}$
10		6.42	7.55	7.66	5.92	4.27	4.22	$10^4$	10360	28365
15		6.87	7.93	8.04	5.17	3.86	3.86	$10^4$	10401	14245
25		7.33	8.26	8.38	4.62	3.07	3.06	$10^4$	68602	11932
50		7.84	8.60	8.72	3.76	2.44	2.50	$10^4$	35127	7102
100		8.24	8.87	9.02	3.11	1.99	2.25	$10^4$	15851	3735
100*		—	—	9.03*	—	—	2.03*	—	—	$10^{4*}$
200		8.57	9.11	—	2.57	1.73	—	$10^4$	8798	—

TABLE I: Velocity and rate of growth of the dispersion of travelling waves in the FIP and AIP model, for different values of  $N_{\text{sat}}$  and  $\kappa$  (in the case of the AIP model). For  $N_{\text{sat}} = 100$  and  $\kappa = 10^{-3}$ , we have also performed a calculation up to  $Y = 4$  only (data denoted by a star) in order to be able to collect enough statistics.

independent of the impact parameter that is considered, Fig. 5. As this is indeed the case, we are free to focus on central impact parameters. Figure 6 shows travelling waves averaged over many events at central impact parameter, for different values of the cutoff  $\kappa$ . (Note that the shape of the front in its forward part is consistent with the theoretical expectation in Eq. (7)). Figures 7 and 8 show the average of the instantaneous velocity and of the dispersion of the front position as a function of the rapidity. Again, a stationary velocity is reached after 1 to 2 units of rapidity. As soon as this regime is reached, the dispersion starts to scale linearly in  $Y$ , as expected.

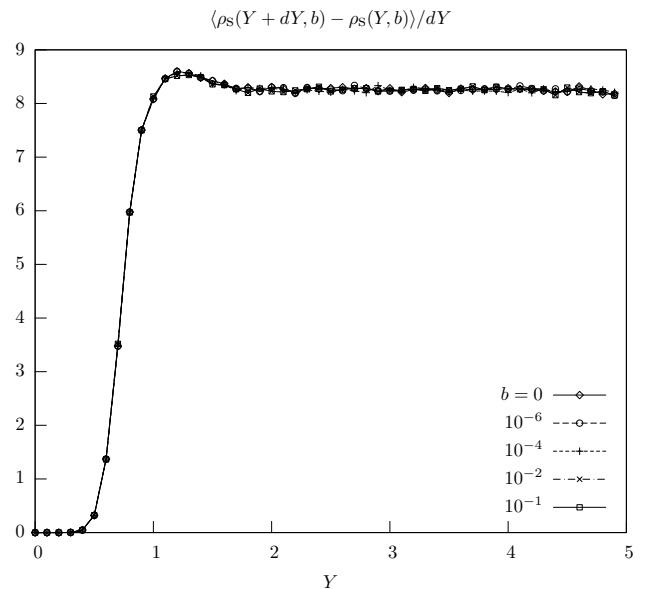


FIG. 5: Instantaneous velocity of the front in the AIP model, for  $N_{\text{sat}} = 25$  and at different impact parameters. The curves are all almost perfectly superimposed.

The diffusion coefficient  $D = d\sigma^2/dY$ , which is the slope of this line, quantifies the amount of fluctuations. The values of the velocity and of the diffusion coefficient are reported in Tab. I, also for different values of  $N_{\text{sat}}$  (and  $\kappa$ ). The numbers have been extracted from a fit between  $Y = 2$  and 5 for the velocity, and between  $Y = 2$  and 4.5 for the diffusion coefficient. We have limited the fit range for the latter<sup>4</sup> to avoid edge effects related to the fact that the far tail of the front sometimes reaches our cut-off on dipole sizes (see *e.g.* Fig. 6), leading to the small turnover for the dispersion observed in Fig. 8.

From Figs. 7 and 8, we already see that there is no strong dependence on the value of  $\kappa$ . To further study this dependence, we have computed the asymptotic velocity for different values of  $\kappa$  and  $N_{\text{sat}} = 25$ . One sees in Fig. 9 a saturation for  $\kappa \lesssim 10^{-3}$  and a very small dependence on  $\kappa$  up to  $\sim 10^{-2}$ , confirming that the cutoff  $\kappa$  does not strongly affect the observables.

There is an important difference between AIP and FIP, where similar results were expected if the hypothesis of local evolution in impact parameter were literally correct. Instead, comparing Figs. 3 and 4 with Figs. 7 and 8, we observe that the FIP model has more fluctuations than the AIP model, as if the effective number of particles were lower, or if some averaging were effectively performed in the AIP evolution. In order to enforce the matching of the velocities and diffusion coefficients of the two models,

<sup>4</sup> Since the velocity instead depends on what happens close to the saturation scale, the fit can safely be extended to  $Y = 5$ .

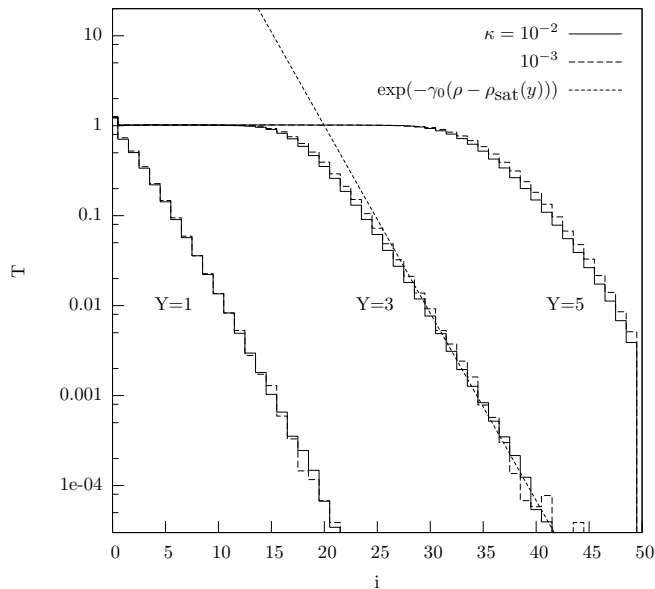


FIG. 6: Average of the event-by-event amplitude in the AIP model as a function of the dipole size at zero impact parameter, for three different rapidities. Two values of the cutoff  $\kappa$  are compared and  $N_{\text{sat}}$  is set to 25.

we should take a value of  $N_{\text{sat}}$  of about 100 for the FIP model, *i.e.* about 4 times that of the AIP model (with  $N_{\text{sat}} = 25$ ). We will try and investigate more systematically this discrepancy below. First, let us examine the correlations between travelling waves at different impact parameters.

### B. Correlations in impact parameter

Fig. 10 represents the correlations between the positions of the wave fronts at different impact parameters in the AIP model, defined as

$$\langle \rho_s(Y, b_1) \rho_s(Y, b_2) \rangle - \langle \rho_s(Y, b_1) \rangle \langle \rho_s(Y, b_2) \rangle. \quad (34)$$

Once again, the different choices of  $\kappa$  lead to very similar results.

We also see very clearly the successive decouplings of the different impact parameters, from the most distant to the closest one, as rapidity increases. Indeed, the correlation functions flatten after some given rapidity depending on the difference in the probed impact parameters, which means that the evolutions decouple. This decoupling is expected as soon as the travelling wave front reaches dipole sizes which are smaller than the distance between the probed impact parameters, *i.e.* at  $Y$  such that  $|b_2 - b_1| \approx 1/Q_s(Y) = B^{-\rho_s(Y)}$ . From the data for  $\rho_s(Y)$ , we can estimate quantitatively the values of the rapidities at which the travelling waves decouple between the different impact parameters. (It is enough to

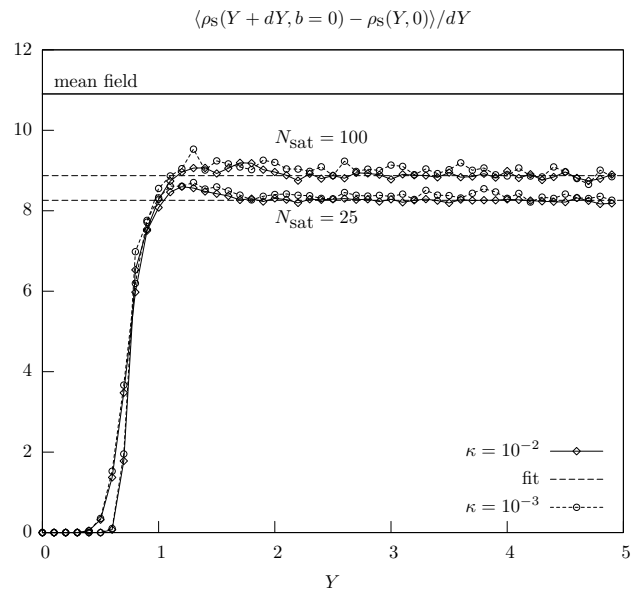


FIG. 7: Instantaneous velocity of the front in the AIP model, for  $N_{\text{sat}} = 25$  and  $N_{\text{sat}} = 100$ , and different values of the cutoff  $\kappa$ . The impact parameter  $b$  is set to 0. The mean-field result is also represented.

invert the above formula for the relevant values of  $b_2 - b_1$ ). These rapidities are denoted by a cross in Fig. 10 for the considered impact parameter differences. Our numerical results for the correlations are nicely consistent with this estimate, since the correlations start to saturate to a constant value precisely on the right of each such cross.

### C. $N_{\text{sat}}$ -dependence and difference between AIP and FIP

We have observed that the travelling wave fronts in the AIP model at a given impact parameter look very much like those appearing in the FIP model, but the parameter  $N_{\text{sat}}$  should be changed by some factor to allow for a matching of their characteristics. In this section, we investigate more quantitatively this point.

To this aim, we compute the front velocity  $V$  and diffusion coefficient  $D = d\sigma^2/dY$  in the AIP model at central impact parameter as a function of  $N_{\text{sat}}$ . We use different values of the cutoff  $\kappa$  (in practice  $\kappa = 10^{-2}$  and  $10^{-3}$ ). A similar calculation can be performed for the FIP model (in this case, there is no cutoff  $\kappa$  to be considered). The results are displayed in Fig. 11.

We notice that the shapes of these curves look similar, in the FIP and AIP model for  $V$  as well as for  $D$ , except maybe for very small values of  $N_{\text{sat}}$  (10 and 15). However, we may superpose the different curves only at the price of performing a rescaling of  $N_{\text{sat}}$  (which corresponds to a shift of the curves on the logarithmic scale chosen in the plot of Fig. 11). Empirically, we find that the AIP model

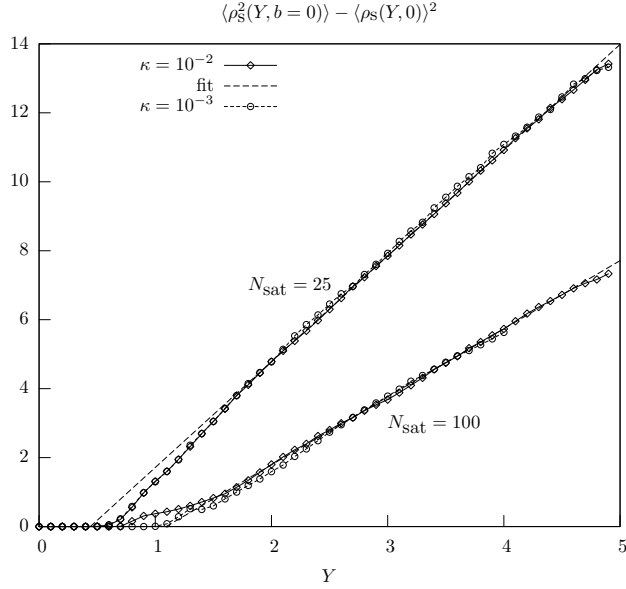


FIG. 8: The same for the variance of the position of the front at central impact parameter. Note that for  $N_{\text{sat}} = 100$  and  $\kappa = 10^{-3}$ , we have data only up to  $Y = 4$ .

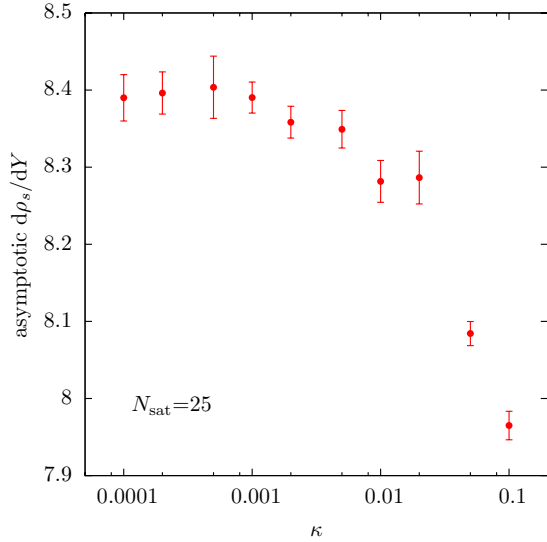


FIG. 9:  $\kappa$  dependence of the asymptotic front velocity for  $N_{\text{sat}} = 25$ .

is equivalent to the FIP model at each impact parameter if one sets  $N_{\text{sat}}$  for the latter about 3.8 times larger than for the former.

We may propose an interpretation of the observed discrepancy. In the course of the evolution, travelling waves at different impact parameters communicate by exchanging dipoles because dipole splitting is not strictly local in coordinate space: starting from any given step, the chain of subsequent splittings extends over an area that is sig-

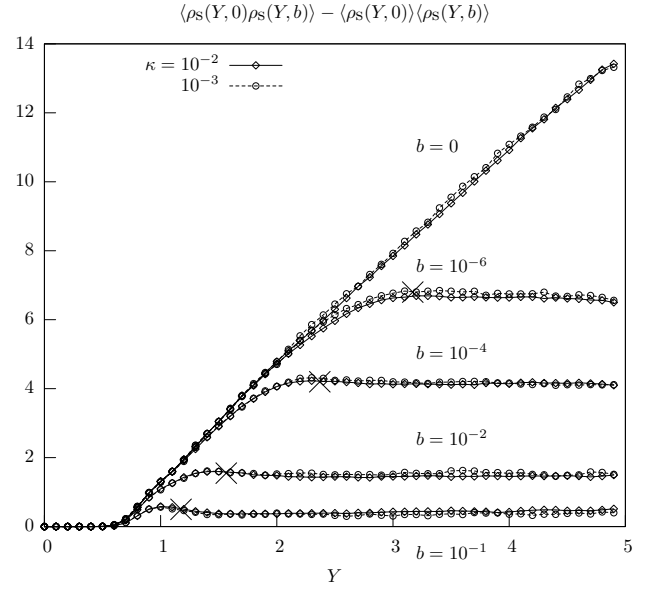


FIG. 10: Correlations between the front position at different impact parameters as a function of the rapidity for  $N_{\text{sat}} = 25$ . The crosses denote the rapidity  $Y$  at which the (inverse of the) saturation scale  $B^{-\rho_s(Y)}$  coincides with the distance in impact parameter space between the probed points.

nificantly larger than the area set by the initial dipole. In this way, the waves may equalise their velocities, and this leads to an extra dynamical averaging with respect to FIP models, at any impact parameter, continuously at any step in the evolution. This effective averaging results in a reduction of the fluctuations in the positions of the waves, and thus to an increase of the front velocity, which becomes closer to the mean-field velocity, and in particular different from the expected velocities in the corresponding one-dimensional travelling wave model (FIP model).

As we have observed in Fig. 11, the scaling factor between  $N_{\text{sat}}$  and the effective maximum number of dipoles in the AIP model seems to be independent of  $N_{\text{sat}}$ . However, we also see that a factor  $\log(N_{\text{sat}})/\gamma_c$  (the length of the front) between AIP and FIP is also consistent with our numerical observation. Unfortunately, we have not been able to find a satisfactory analytic explanation for this factor.

In any case, since we find that the discrepancy amounts to a simple rescaling of  $N_{\text{sat}}$  by a constant or a slowly varying factor (at least in the range of the values of  $N_{\text{sat}}$  that we were able to explore), it is likely that it is a sub-leading effect, and that the AIP and FIP models would agree asymptotically for large  $N_{\text{sat}}$ . Hence we do not think that this slight mismatch between the AIP and the FIP models spoils in any way the one-dimensional reaction-diffusion picture of high-energy scattering.

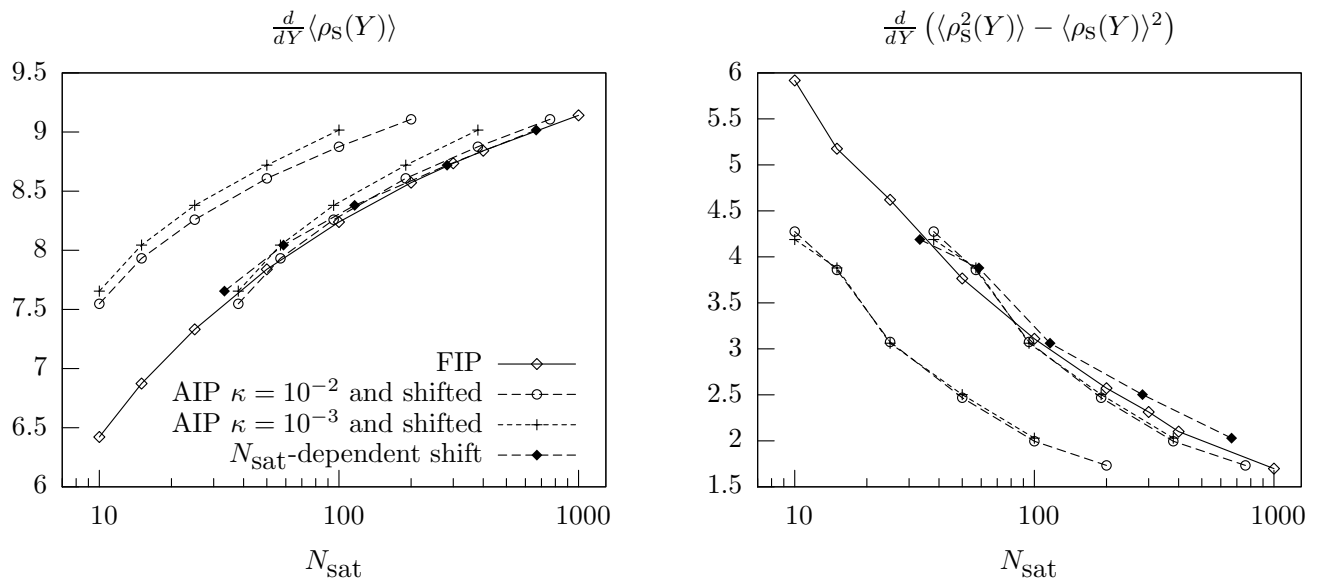


FIG. 11: Steady-regime velocities (left) and diffusion coefficients (right) of the wave front in the FIP model (full lines) and at central impact parameter in the AIP model (dashed and dotted lines). The two leftmost curves in each plot correspond to the actual results of the calculation; The two rightmost ones are the same but shifted. The shift is a scaling factor of  $N_{\text{sat}} = 1/\alpha_s^2$  equal to 3.8. The curves with filled black squared correspond to the AIP model shifted by  $\frac{1}{\gamma_c} \log N_{\text{sat}}$ . For  $N_{\text{sat}} = 100$  and  $\kappa = 10^{-3}$ , we have performed a fit up to  $Y = 4$  only (see Tab. I).

## V. CONCLUSION

One condition for high-energy evolution in QCD to be in the universality class of a one-dimensional reaction-diffusion processes is that the partonic evolution remains local in impact-parameter space. In this paper, with the help of a toy model (called ‘‘AIP’’) engineered to incorporate the essential features of QCD and to be manageable numerically, we have checked that this is indeed the case. We have measured the properties of travelling waves at given impact parameters, and showed that the correlations between waves at different points in coordinate space vanish when the rapidity gets large enough, as expected for a local evolution.

Furthermore, we have compared the properties of the travelling waves that appear in this model with the features of their counterparts in a model that has no impact parameter dependence (called ‘‘FIP’’), but which is identical to the former in all other respects. We have found that the results are similar, except that the number of partons at saturation should be larger by a factor of the order of 4 in the FIP model, suggesting that the latter has more fluctuations. It is also plausible that this factor has a slow  $N_{\text{sat}}$ -dependence and may vary like  $\frac{1}{\gamma_c} \log N_{\text{sat}}$ . At this stage, our numerical data do not enable us to check whether one of these guesses is literally correct.

We do not have a final explanation for the discrepancy between the AIP and FIP models yet. However, the fact that the factor by which  $N_{\text{sat}}$  should be scaled for the matching to occur does not exhibit a strong  $N_{\text{sat}}$ -

dependence (remember that  $N_{\text{sat}} \sim 1/\alpha_s^2$  in QCD) leads us to think that it is a subleading effect in the large- $N_{\text{sat}}$  (small- $\alpha_s$ ) limit, and thus, that the one-dimensional reaction-diffusion picture is indeed valid, up to the relevant replacement of the parameter  $N_{\text{sat}}$  by some effective number of particles relevant to the propagation of the travelling waves, yet to be understood more precisely.

Note that, though a full study with two transverse degrees of freedom would be of great interest, we believe that our one-dimensional picture grasps the important aspects of the problem and, based on universal properties of the reaction-diffusion systems, we expect our results to hold for full QCD.

Finally, we can think of several other improvements beyond our study. We have considered only one saturation mechanism, which consisted in merely vetoing parton splittings in phase space cells already occupied by at least  $N_{\text{sat}}$  particles. We could try and check whether other saturation mechanisms (such as parton recombination) would bring about more correlations in impact parameter. It would also be desirable to achieve some analytical understanding, in particular of the rescaling factor between the AIP and FIP model. To this aim, it may be interesting to study the chains of successive dipole splittings in the AIP model, in order to find out whether rare fluctuations spread in a wider-than-expected area in impact parameter.

### Acknowledgments

The work of S.M. is supported in part by the Agence Nationale pour la Recherche (France), contract ANR-06-JCJC-0084-02. G.S. is supported by Contract No. DE-

AC02-98CH10886 with the U.S. Department of Energy. We thank the Galileo Galilei Institute for Theoretical Physics for the hospitality and the INFN for partial support when this work was being initiated.

- 
- [1] L. V. Gribov, E. M. Levin and M. G. Ryskin, Phys. Rept. **100**, 1 (1983).
  - [2] A. H. Mueller and J. W. Qiu, Nucl. Phys. B **268**, 427 (1986).
  - [3] I. Balitsky, Nucl. Phys. B **463**, 99 (1996).
  - [4] Y. V. Kovchegov, Phys. Rev. D **60**, 034008 (1999); Phys. Rev. D **61**, 074018 (2000).
  - [5] J. Jalilian-Marian, A. Kovner, A. Leonidov and H. Weigert, Nucl. Phys. B **504**, 415 (1997); Phys. Rev. D **59**, 014014 (1998); E. Iancu, A. Leonidov and L. D. McLerran, Phys. Lett. B **510**, 133 (2001); Nucl. Phys. A **692**, 583 (2001); H. Weigert, Nucl. Phys. A **703** (2002) 823.
  - [6] For a review and more references on the JIMWLK formalism, see H. Weigert, Prog. Part. Nucl. Phys. **55**, 461 (2005).
  - [7] S. Munier and R. Peschanski, Phys. Rev. Lett. **91**, 232001 (2003); Phys. Rev. D **69**, 034008 (2004); Phys. Rev. D **70**, 077503 (2004).
  - [8] A. H. Mueller and A. I. Shoshi, Nucl. Phys. B **692**, 175 (2004).
  - [9] E. Iancu and D. N. Triantafyllopoulos, Nucl. Phys. A **756**, 419 (2005), Phys. Lett. B **610** (2005) 253.
  - [10] A. Kovner and M. Lublinsky, Phys. Rev. Lett. **94** (2005) 181603
  - [11] Y. Hatta, E. Iancu, L. McLerran, A. Stasto and D. N. Triantafyllopoulos, Nucl. Phys. A **764** (2006) 423
  - [12] E. Iancu, A. H. Mueller and S. Munier, Phys. Lett. B **606**, 342 (2005).
  - [13] For a reviews on the FKPP equation and its stochastic extensions, see W. Van Saarloos, Phys. Rep. **386**, 29 (2003); D. Panja, Phys. Rep. **393**, 87 (2004).
  - [14] A. H. Mueller, Nucl. Phys. B **415**, 373 (1994).
  - [15] G. P. Salam, Nucl. Phys. B **461**, 512 (1996).
  - [16] G. P. Salam, Comput. Phys. Commun. **105**, 62 (1997).
  - [17] A. H. Mueller and G. P. Salam, Nucl. Phys. B **475**, 293 (1996).
  - [18] E. Avsar, G. Gustafson and L. Lonnblad, JHEP **0507** (2005) 062; JHEP **0701** (2007) 012.
  - [19] G. Soyez, Phys. Rev. D **72** (2005) 016007
  - [20] R. Enberg, K. J. Golec-Biernat and S. Munier, Phys. Rev. D **72**, 074021 (2005).
  - [21] E. Iancu, G. Soyez and D. N. Triantafyllopoulos, Nucl. Phys. A **768**, 194 (2006).
  - [22] E. Iancu, J. T. de Santana Amaral, G. Soyez and D. N. Triantafyllopoulos, Nucl. Phys. A **786** (2007) 131.
  - [23] L. N. Lipatov, Sov. J. Nucl. Phys. **23**, 338 (1976); E. A. Kuraev, L. N. Lipatov, and V. S. Fadin, Sov. Phys. JETP **45**, 199 (1977); I. I. Balitsky and L. N. Lipatov, Sov. J. Nucl. Phys. **28**, 822 (1978).
  - [24] A. H. Mueller, A. I. Shoshi and S. M. H. Wong, Nucl. Phys. B **715**, 440 (2005).
  - [25] K. J. Golec-Biernat, L. Motyka and A. M. Stařto, Phys. Rev. D **65**, 074037 (2002).
  - [26] A. H. Mueller and D. N. Triantafyllopoulos, Nucl. Phys. B **640**, 331 (2002).
  - [27] A. M. Stařto, K. J. Golec-Biernat and J. Kwiecinski, Phys. Rev. Lett. **86**, 596 (2001).
  - [28] E. Brunet, B. Derrida, Phys. Rev. E **56**, 2597 (1997); Comp. Phys. Comm. 121-122 (1999) 376; J. Stat. Phys. 103 (2001) 269.
  - [29] E. Brunet, B. Derrida, A. H. Mueller and S. Munier, Phys. Rev. E **73**, 056126 (2006).
  - [30] D. Y. Ivanov, R. Kirschner, E. M. Levin, L. N. Lipatov, L. Szymanowski and M. Wusthoff, Phys. Rev. D **58**, 074010 (1998).
  - [31] M. Ciafaloni, D. Colferai and G. P. Salam, JHEP **9910** (1999) 017.
  - [32] See *e.g.* GMP, The GNU Multiple Precision Arithmetic Library, <http://gmplib.org/>.